applied sciences

MDPI

Article

Estimation of Shallow Shear Velocity Structure in a Site with Weak Interlayer Based on Microtremor Array

Cong Jin [1,2,3], Song Lin [1,2,3,*], Jing Wang [4], Hongwei Zhou [1,2,3] and Miao Cheng [1,2,3]

1 Hubei Key Laboratory of Earthquake Early Warning, 40 Hongshance Road, Wuhan 430071, China
2 Hubei Earthquake Agency, 48 Hongshance Road, Wuhan 430071, China
3 Wuhan Institute of Earthquake Engineering Co., Ltd., 40 Hongshance Road, Wuhan 430071, China
4 School of Civil Engineering, Shijiazhuang Tiedao University, N 2st Ring E Road, Shijiazhuang 050043, China
* Correspondence: ls6102212@163.com

Abstract: A site condition survey is extremely important for the seismic fortification of major projects. The distribution of underlying weak interlayer in sites is extremely harmful to buildings. However, it is a technical problem to find out the distribution of weak interlayer in the overburden. The shallow velocity structure can directly reflect the change characteristics of a stratigraphic structure. In this paper, acquisition of background noise is conducted using a microtremor linear array method, and the distribution characteristics of two typical stratigraphic structures in Wuhan, Hubei Province, are obtained through an inversion of the apparent S-wave velocity; meanwhile, the equivalent shear-wave velocity and the overburden thickness are estimated, which provides a basis for site classification. The research results are as follows: (1) The two-dimensional profile of the apparent S-wave velocity obtained by the microtremor linear array method can be used for fine imaging of the stratum with weak interlayer, and its distribution form and velocity structure characteristics are highly consistent with those of the drilling data. (2) Compared to the borehole data obtained through in situ test, the error of the overburden thickness and the equivalent shear-wave velocity estimated by the inversion of the apparent S-wave velocity is only about 10%, and the estimated parameters can be directly used for site classification. These results can provide important parameters for seismic fortification of major projects, and also provide reference for the exploration of unfavorable geological bodies, such as weak interlayer in complex urban areas, in the future, which can have good scientific significance and popularization value.

Keywords: microtremor array; weak interlayer; engineering site; equivalent shear wave velocity; site category

Citation: Jin, C.; Lin, S.; Wang, J.; Zhou, H.; Cheng, M. Estimation of Shallow Shear Velocity Structure in a Site with Weak Interlayer Based on Microtremor Array. *Appl. Sci.* **2023**, *13*, 185. https://doi.org/10.3390/app13010185

Academic Editor: Arcady Dyskin

Received: 24 November 2022
Revised: 19 December 2022
Accepted: 21 December 2022
Published: 23 December 2022

1. Introduction

Earthquake has accompanied the development of human society all along and has caused huge loss of life and property. A large number of earthquake damage data show that site conditions are very sensitive to earthquake phenomena and earthquake damage level, and the covering soil layer, surface topography, and bedrock surface of local sites become the direct factors for the distribution of earthquake disasters [1]. The shallow shear-wave velocity is one of the most important parameters for the description of engineering sites. Understanding the underground shear-wave velocity structure is the basis for conducting surface seismic impact analysis, evaluating seismic effect, and carrying out engineering earthquake resistance of local sites, which is of great significance for earthquake disaster prediction and prevention [2]. Ground motion intensity is closely related to soil category and nature, and overburden thickness. Understanding the structural characteristics of shallow surface is essential for the study of seismic site effect, especially when the overburden of a site is thick and the site contains a thick weak interlayer, its overall stiffness is small [3] and its stress distribution is not safe for operation under seismic loading [4].

Meanwhile, a weak interlayer can amplify low-frequency signal, which will seriously affect the peak acceleration and characteristic period of the ground motion, causing great harm to engineering projects. Therefore, it is particularly important to carry out a detailed survey on sites with weak interlayer in general, as well as a survey of urban seismic risk.

In traditional engineering investigation, the conventional methods to obtain the shallow shear-wave velocity mainly include the cross-(single-)hole method and Rayleigh wave exploration [5]. It is generally considered that more accurate velocity values can be obtained by the cross-(single-)hole method. However, only the shear-wave velocity structure of the strata near boreholes can be obtained, which indicates that it will cost a lot of labor and time to obtain the velocity structure change of the whole site. In comparison, The Rayleigh wave exploration is a nondestructive testing method by which some results have been achieved in detecting low-velocity weak interlayer [6]. However, the currently accepted rule of thumb of the maximum penetration depth is approximately half the longest wavelength [7], and the effective exploration depth should be less than the maximum penetration depth of Rayleigh waves [8].

In recent years, microtremor survey has become one of the research hotspots in geophysical exploration [9] at home and abroad, due to such advantages as signal acquisition from natural sources, wide-frequency band, large detectable depth, and freedom from urban noise interference, and it has been rapidly developed with the development of processing technology and accumulation of observation data. There are two methods for microtremor survey, namely the horizontal-to-vertical spectral ratio (HVSR) [10] method and multichannel analysis [11] method. Research [12,13] shows that, using the multichannel analysis based on the microtremor array method, the shallow shear-wave velocity can be obtained, and the sediment thickness or bedrock depth can be divided, with very high accuracy especially for hard rock covered with sediment [14]. The microtremor array method has been widely used in densely populated urban areas [15,16] due to its versatility and convenient operation. Xu [17] applied the microtremor array method to urban rail transit. By conducting a fine exploration of the stratum within the depth of 50 m, they solved geological problems, such as boulders, karst, cracks, fault fracture zones, and soil-rock interface in an urban geological survey. Tian [18] took the geothermal resource area in the south of Jiangsu Province as an example to develop effective stratification within a depth of 2.5 km by adjusting the array radius. Compared with the borehole results, the depth error is small. Many research studies [19,20] show that effective surveyed depth using this method ranges from tens of meters on the surface to several kilometers in the shallow crust.

However, at present, there are few research studies using a microtremor survey for weak interlayer, and the results are not satisfactory. On the other hand, in engineering, the equivalent shear-wave velocity and overburden thickness are obtained generally by drilling, and "site category" is defined according to anti-seismic design specifications to consider the impact of local site conditions on site effects. In this paper, based on two typical stratigraphic models in the Wuhan area and through a theoretical study of the long-spread microtremor linear array, the data obtained are analyzed in detail and good results are achieved in delicately depicting the shallow shear-wave velocity structure, dividing the low-velocity weak interlayer, and estimating the equivalent shear-wave velocity and overburden thickness. The feasibility and effectiveness of this method are verified by calibration and comparison with borehole data. Furthermore, with its convenience and efficiency of field operation, this method helps to reduce the drilling cost to a certain extent.

2. Geological Background

Wuhan is located between the Dabieshan hills in the northeast of Hubei Province and the Mufu hills in the southeast, and in the east of Jianghan Plain. Its territory is high in the east and south and low in the west and north, and the middle is divided into Wuchang, Hankou, and Hanyang sections by the Yangtze River and the Hanjiang River in the shape of a "U". The landform in the urban area is mainly plain, with a small number of low mountains, hills, and heights. The flat plain is formed by the flood siltation of the Yangtze

River, the Hanshui River, and other tributaries, and distributed along both banks of rivers and around lakes, as shown in Figure 1.

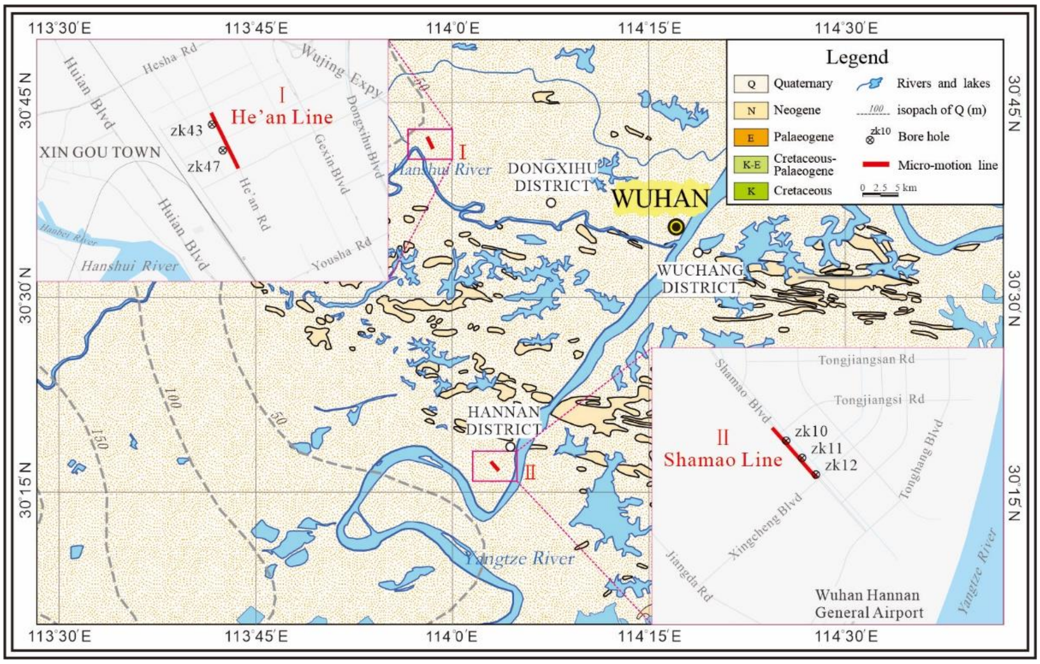

Figure 1. Location of survey lines in the study area.

Geologically, Wuhan is located in the composite part of the west wing of the Huaiyang epsilon-type front arc and the Neocathaysian tectonic system, and also in the second Neocathaysian subsidence zone on an epsilon-type structure. The structural traces left by the Yanshan movement in this area indicate that the main compressive stress here is in the near north-south direction, so a series of near east-west compressive structural planes and the accompanying near east-west compressive faults, as well as the NNW and NNE compressive torsional and tensional-torsional faults, are formed. Since later and more recent periods, the regional structure has changed to the Neocathaysian system as the main body, and with the northeast Yangtze River as the boundary, the Hankou section in the west belongs to the northeast edge of the Jianghan-Dongting fault depression, and the Wuchang section in the east belongs to the edge of the lower Yangtze depression. In terms of landform, the Hankou section in the west is located at the northeast edge of the Jianghan-Dongting settlement area, and the Wuchang section in the east is located at the Huangshi-Xianning undulating lifting area. Since the end of the Middle Pleistocene, river and lake terraces of Class II~III have been widely developed in Wuchang and Hanyang, and the Dongxihu area in Hankou has become a buried terrace.

The landforms of the study area are flat plains. According to previous drilling and geological data, the overburden of study area I is composed of silty clay, fine silt, sand, and pebble layers of the Quaternary Holocene alluvium. The entire overburden is generally 40~50 m thick, with the maximum thickness of about 80 m. The deep bedrock is Cretaceous-Paleogene conglomerate. The overburden of study area II is formed by the artificial accumulation and alluvial-proluvial accumulation of the Holocene series. The upper fine-particle layer is mainly silty clay, partially mixed with silt and silty sand, and the lower coarse-particle layer is mainly silty fine sand and medium coarse sand, and partially silt and gravel. The thickness of the entire overburden varies from 60 to 90 m, and the deepest layer is more than 100 m. The deep bedrock is Cretaceous-Paleogene argillaceous siltstone.

3. Method

3.1. Microtremor Array Method

Microtremor array method [21] is developed on the basis of background noise imaging, and it refers to the way to extract surface waves from a group of weak-vibration signals (number of stations ≥ 2) without a specific source, analyze their dispersion characteristics, and obtain the velocity structure of the underground strata through an inversion of the dispersion curves. Microtremor signal is a complex one composed of body wave (longitudinal wave and transverse wave) and surface wave (Rayleigh wave and Love wave). Surface wave energy accounts for more than 70% of the total signal energy [22]. Microtremor signal is from both natural phenomena, such as air pressure, wind speed, waves, and tidal changes, and vehicle movement, machine operation, and people's daily production and life. Therefore, this method is not interfered by urban electromagnetic environment and cultural and industrial activities and is a new way for a detailed detection of urban underground space.

The commonly used array types are generally regular and irregular ones. The regular type includes linear array (such as linear array, "T" array, and "L" array) and circular array (including triangle array and "cross" array which can be regarded as special circular array). The phase velocity obtained by triangular and linear arrays are in good agreement with each other [23]. Circular array is conducive to receiving random microtremor information from different directions, which can ensure the accuracy of dispersion curves to a certain extent. However, in densely populated urban areas, the existing infrastructure will limit the distribution of two-dimensional array. Although noise resistance of linear array is weak due to its azimuth directivity, in urban geophysical exploration with limited sites, rich environmental noise can basically meet the condition that surface wave covers all directions, providing a theoretical basis for the long-spread linear microtremor array method.

3.2. Spatial Autocorrelation Method

The method of extracting dispersion curves from microtremor signal can be traced back to the 1960s. Aki proposed the theory of spatial autocorrelation (SPAC) [24]. Since then, research based on microtremor has gradually developed from theory to practical application, and other methods of extracting dispersion curves, such as the frequency-wavenumber (FK) spectrum method [25] and the method of multi-channel analysis of surface waves (MASW) [26], have also been developed. In recent years, through improving the algorithm, researchers have proposed multi-channel analysis of passive surface waves (MAPS) [27], pseudo-linear-array analysis of passive surface waves (PLAS) [28] and phase-weighted stacking (PWS) method [29], and have achieved good results in some typical cases.

According to the SPAC method, the natural microtremor signal in a certain period of time is a sample function $X(t, \xi(x, y))$ of a stationary random process, and its spectrum can be expressed as follows:

$$X(t, \xi(x, y)) = \oint\!\!\oint \exp(i\omega t + iK\xi) dZ(\omega, K) \tag{1}$$

where $\omega = 2\pi f$ is the angular frequency; $K = (k_x, k_y)$ is the wave-number; and Z is the orthogonal random process.

The SPAC method generally adopts circular array, with one station at the center of the circle and other ones at the circumference. After normalization of the power spectral density of the incident noise field, with maintenance of the circumference radius and change of the frequency, the spatial autocorrelation coefficient of average azimuth is as follows:

$$\rho(\omega, r_0) = J_0(r_0 \cdot \omega / c(\omega)) \tag{2}$$

where J_0 is the Bessel function of class I of zero order. It can be seen that the spatial autocorrelation coefficient obtained on circular array with radius r is related to the frequency and changes in the form of Bessel function of class I of zero order. Therefore, the dispersion curve of phase velocity $c(\omega)$ can be obtained by calculating the spatial autocorrelation coefficient ρ between the center point of the circular array and the points at the circumference and fitting it with the zero-order Bessel function.

Extended spatial autocorrelation (E-SPAC) keeps the frequency and changes the circumference radius, and, thus, (2) is expressed as follows:

$$\rho(\omega_0, r) = J_0(r \cdot \omega_0 / c(\omega)) \tag{3}$$

From the above formula, the relationship between the autocorrelation coefficient and the distance r can be obtained, which makes it possible to process irregular array. Compared to the SPAC method, the layout of field arrays is more flexible [30]. In this paper, the more widely used E-SPAC method is adopted for extracting surface-wave dispersion energy with a higher resolution from microtremor signal.

4. Applications to Field Data

In this paper, two typical stratigraphic models in the Wuhan area are taken as the research object for microtremor measurement and analysis. The layout of the survey lines and the distribution of the boreholes nearby are shown in Figure 1.

The He'an Line in study area I is located in the Dongxihu District of Wuhan City, in the north of the Yangtze River, where the Hanjiang River, the Hanbei River, and the Fuhuan River meet and surround. The landform of this district is mainly low plain accumulated by rivers and lakes, with flat terrain. According to the results of a previous drilling, field in situ test and an indoor geotechnical test, the shallow stratum velocity model of the site is of an increasing type.

The Shamao Line in study area II is located in the Hannan District in the southwest suburb of Wuhan City, bounded by the Yangtze River in the east and south. The landform of this district is mainly river alluvial plain and wide plain formed by lake deposition, with flat terrain. According to previous drilling data of the site, there is a layer of plastic silt mixed with silty clay in between medium-coarse sand mixed with gravel and underlying argillaceous siltstone, with thickness of about 20 m. According to the results of a previous field in situ test and an indoor geotechnical test, the shallow stratum velocity model of the site is of a low-velocity interlayer type.

4.1. Data Acquisition

A total of 50 ALLSEIS-1C/LF broadband seismic stations produced by Beijing Zhongke Shenyuan Science and Technology Co., Ltd. (Beijing, China) are used for microtremor data acquisition, with built-in detectors of broadband (1–240 Hz) and high sensitivity. Long-spread linear array is selected, with station spacing of 5 m, exploration point spacing of 5 m, sampling rate of 4 ms, and sampling duration of 30 min. During the field work, 50 stations are deployed at one time along a linear survey line using the roll-along acquisition mode. After 30 min of stable acquisition, the stations continue to roll forward to complete profile measurement (see Figure 2). The layout in this way is more convenient and efficient for microtremor survey in complex urban areas with limited sites.

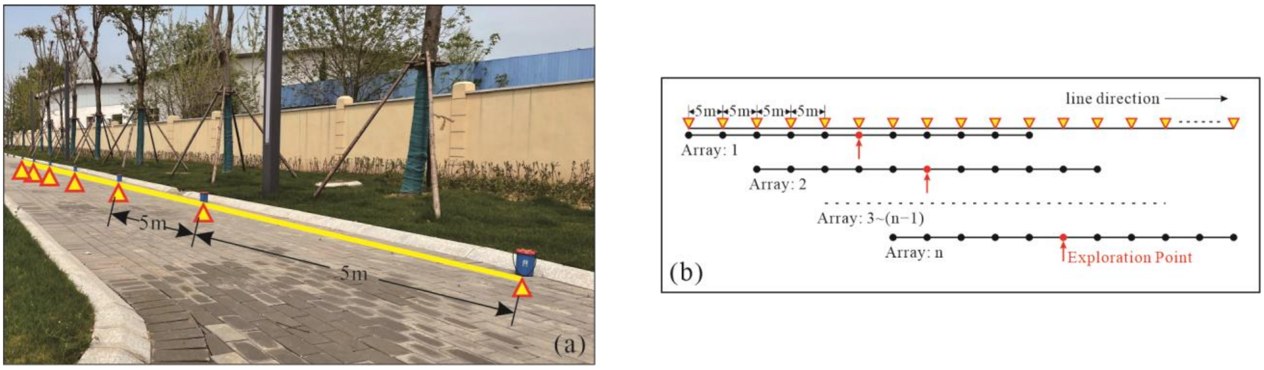

Figure 2. Schematic layout of the microtremor linear array. (**a**): photographs of field work; (**b**): diagram of the roll-along acquisition mode.

During data pre-processing, several station signals are formed into an array with the exploration point as the center according to the depth of the target layer, and the dispersion curve is extracted by the E-SPAC method. The number of stations in the array can be determined according to the principle of H = (3–5) × R [21] between the detection depth H and the array radius R. Through an inversion of the dispersion curve of a certain exploration point, the apparent S-velocity structure of the underground medium can be estimated, and, finally, the pseudo-2D profile of the apparent S-wave velocity under the survey lines can be obtained.

4.2. Data Processing

For data processing of the He'an Line, 13 consecutive stations are selected for each exploration point to form a linear array, with an effective exploration depth of about 100 m. In order to fully illustrate the effectiveness of fine detection by the microtremor array method, the exploration points near the boreholes are used as an example. The spatial autocorrelation coefficients of some different frequencies obtained from the microtremor records at point H32 near borehole zk43 are shown in Figure 3.

The frequency–velocity diagram can be obtained by fitting the first kind of zero-order Bessel function as shown in Figure 4a. The dispersion energy is relatively concentrated within the frequency range of 1.8–16 Hz. The extracted dispersion curve is the line of black dots in the figure, which is smooth and continuous. The initial model is established according to the site borehole data, and an inversion of the extracted dispersion curve is conducted. The inversion curve is shown in the line of red triangles in Figure 4a, and the fitting matching degree is about 93.1%.

The inversion apparent S-wave velocity model is shown in the red dotted line in Figure 4b. According to the inversion result, the apparent S-wave velocity varies between 170–196 m/s within the depth range of 0–22.5 m. As seen from the core photo of borehole zk43 in Figure 5, this layer is mainly composed of silty clay (plastic) and silty fine sand (slightly dense). From 22.5 m to 49.6 m, the apparent S-wave velocity gradually increases to 314 m/s, and the main components are silty fine sand (moderately dense), medium sand (dense), and sand mixed with pebbles. The underlying bedrock is conglomerate. The apparent S-wave velocity of the stratum below 49.6 m depth is greater than 543 m/s. According to the *Code for Seismic Design of Buildings* (GB 50011-2010), the shear-wave velocity of 500 m/s is defined as the boundary of soil and rock. Thus, it can be determined that the overburden thickness is about 55.8 m, which is of little difference from the depth of 51.8 m of the moderately-weathered conglomerate roof revealed by borehole zk43. The field in situ test result is shown in Figure 4b, where the blue dotted line is the shear-wave velocity curve per meter, and the black solid line is the average layer-wave velocity, which is basically consistent with the change trend of the inversion apparent S-wave velocity model.

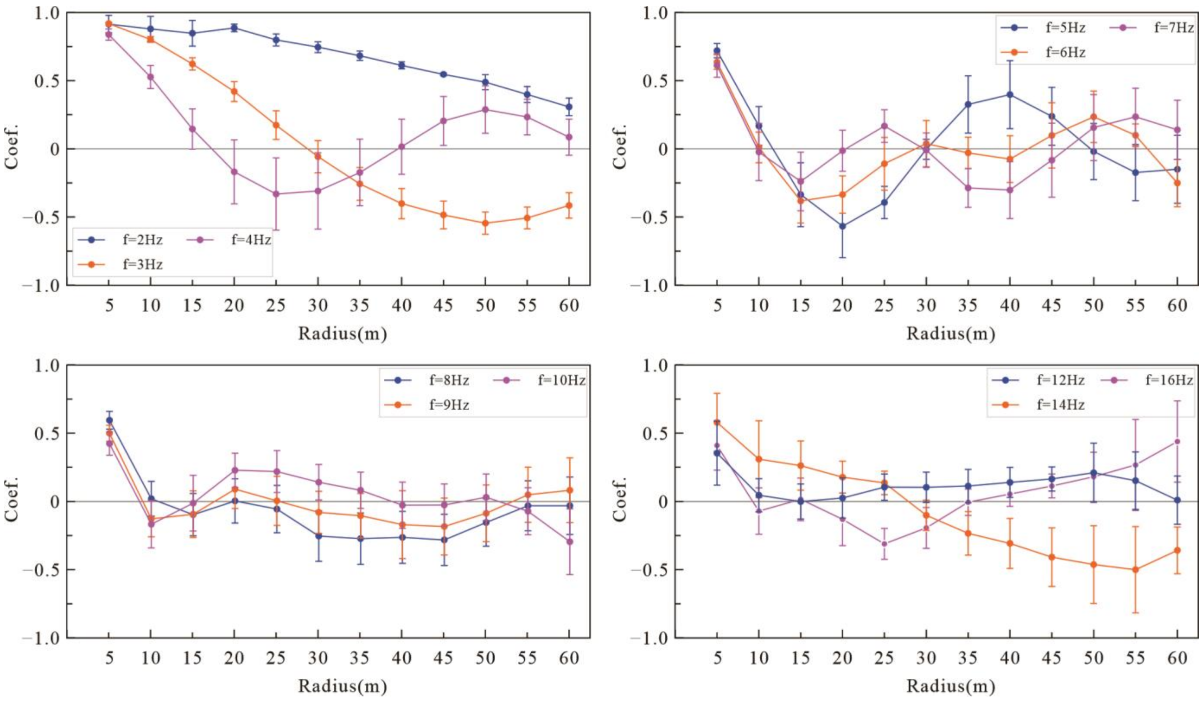

Figure 3. Autocorrelation coefficient of partial frequency at point H32.

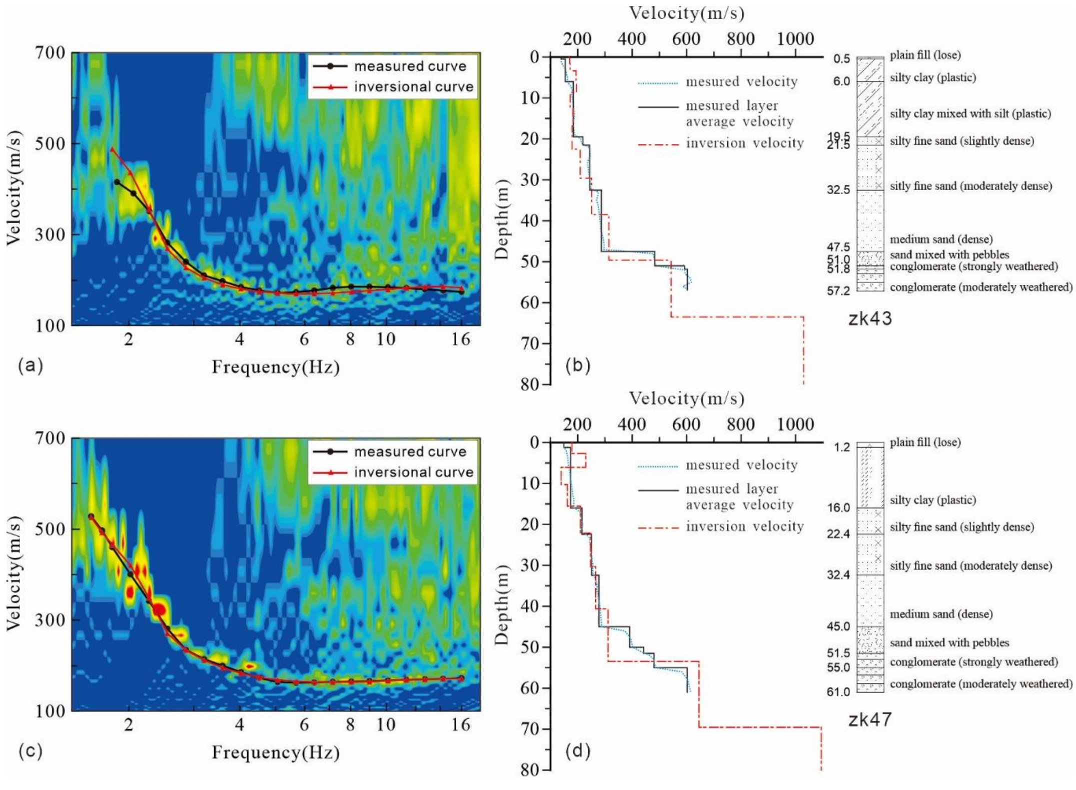

Figure 4. Dispersion curves and inversion results of microtremor exploration points in study area I. (**a**) dispersion curves of H32; (**b**) inversion model of H32 and in situ test results of zk43; (**c**) dispersion curves of H110; and (**d**) inversion model of H110 and in situ test results of zk4.

Figure 5. Core sample photos of borehole zk43.

Similarly, the measured and inversion dispersion curves of exploration point H110 near borehole zk47 are shown in Figure 4c, and the fitting matching degree is about 97.2%. The apparent S-wave velocity below 53.5 m of the inversion model is greater than 645 m/s. Thus, it can be determined that the overburden thickness is about 57.2 m, which is of little difference from the depth of 55.0 m of the moderately-weathered roof revealed by the borehole. In Figure 4d, the change trend of the average layer-wave velocity obtained from the field in situ test is consistent with that of the inversion apparent S-wave velocity model, with high consistence especially in the depth range of 10.2–40.6 m. The application effect of the above conventional velocity model of increasing type further verifies the effectiveness of the microtremor array method in detecting shallow velocity structure.

For data processing of the Shamao Line, 21 stations are selected to form a linear array, with an effective detection depth of about 150 m. The results are shown in Figure 6.

Point S33 of the Shamao Line is located near borehole zk10. Figure 6a shows the dispersion energy of exploration point S33 obtained by the E-SPAC method. The dispersion energy is relatively concentrated within the frequency range of 1.2–16 Hz. The extracted dispersion curve is the line of black dots in the figure, which is smooth and continuous. The initial model is established mainly based on the site borehole data, and a low-velocity layer with a shear-wave velocity of 250 m/s is set at the depth of 50–70 m. An inversion of the extracted dispersion curve is conducted and the result is shown in the line of red triangles in Figure 6a, and the fitting matching degree is about 96.8%.

The inversion apparent S-wave velocity model is shown in the red dotted line in Figure 6b. The apparent S-wave velocity varies between 185–202 m/s within the depth range of 0–31.9 m. As seen from the core photo of borehole zk10 in Figure 7, this layer is mainly composed of muddy silty clay mixed with silt (soft plastic) and silty clay (plastic). Below the layer are silty fine sand (slightly-moderately dense), medium coarse sand with gravel, and pebbles (moderately dense-dense), and the apparent S-wave velocity gradually increases to 359 m/s from 31.9 m to 57.6 m. There is a low-velocity interlayer between depth of 57.6 and 73.3 m and the inversion apparent S-wave velocity is about 298 m/s; the lithology revealed by the borehole is silt mixed with silty clay (plastic), and the depth is 57.8–73.3 m, with which the inversion model is highly consistent. The underlying layer is strongly-weathered argillaceous siltstone. The apparent S-wave velocity gradually increases to 498 m/s, and is greater than 770 m/s below the depth of 110.0 m. Thus, it is speculated to be moderately-weathered argillaceous siltstone. The overburden thickness is about 93.7 m according to the specifications. The field in situ test results are shown in

Figure 6b, where the blue dotted line is the shear-wave velocity curve per meter, and the black solid line is the average layer-wave velocity, which is consistent with the change trend of the inversion apparent S-wave velocity model. The wave velocity value is highly consistent with the stratification depth.

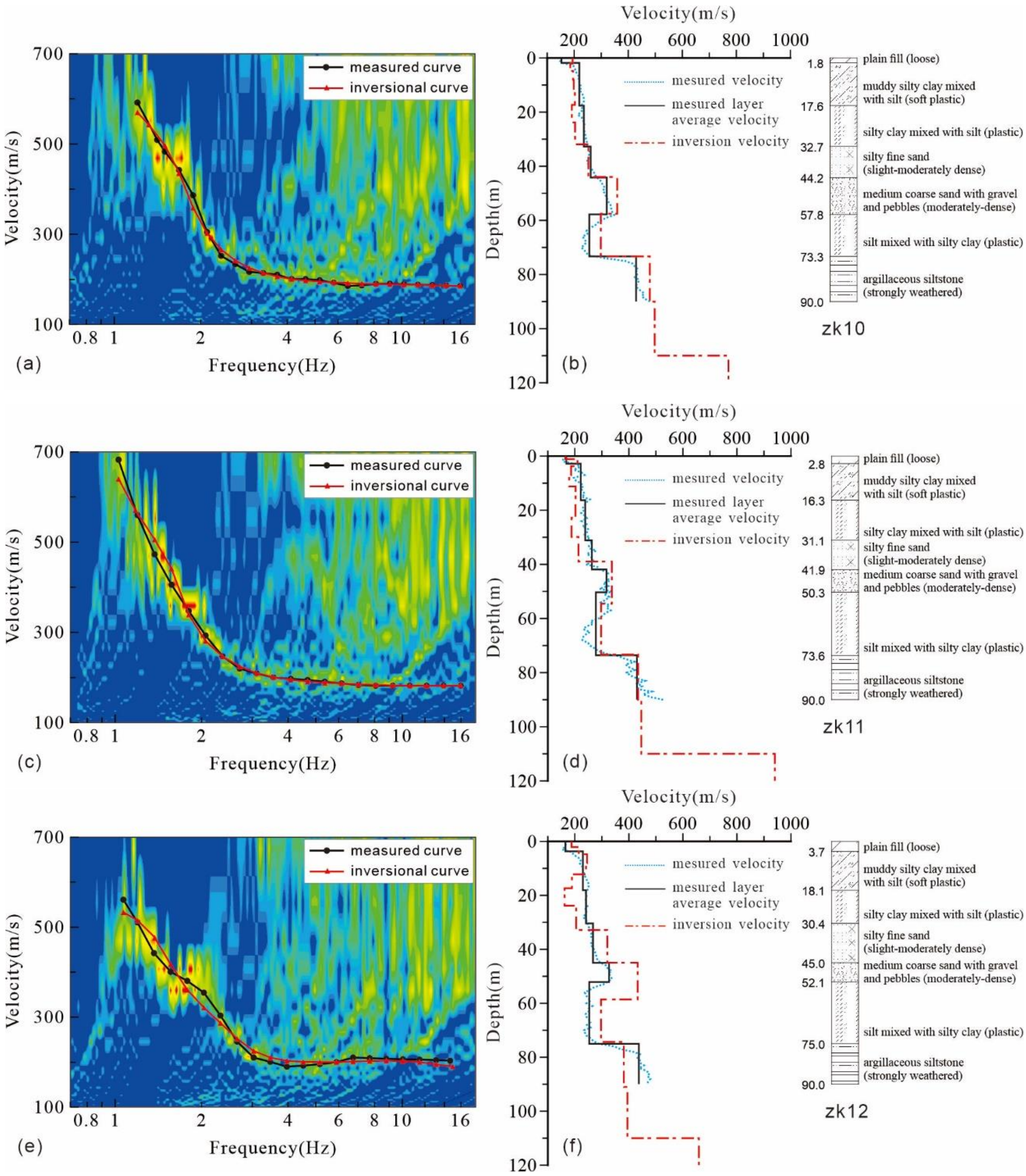

Figure 6. Dispersion curves and inversion results of microtremor exploration points in study area II. (**a**) dispersion curves of S33; (**b**) inversion model of S33 and in situ test results of zk10; (**c**) dispersion curves of S95; (**d**) inversion model of S95 and in situ test results of zk11; (**e**) dispersion curves of S151; and (**f**) inversion model of S151 and in situ test results of zk12.

Figure 7. Partial core sample photos of borehole zk10.

Similarly, the measured and inversion dispersion curves of exploration points S95 and S151 are shown in Figure 6c,e, with the fitting matching degree of about 96.5% and 91.9%, and the overburden thickness of about 101.0 m and 107.6 m, respectively. The microtremor inversion velocity model reflects well the distribution of low-velocity interlayer, which, for exploration point S95, is at the depth of 54.6–73.3 m, and, for exploration point S151 point, is at 58.6–74.3 m, As shown in Figure 6d,f; for both, the apparent S-wave velocity is about 297 m/s, which is consistent with the depth range of the layer revealed by the nearby boreholes zk11 and zk12. These results fully prove that weak interlayer can be well identified by the method.

4.3. Estimation of Equivalent Shear-Wave Velocity

As an important dynamic parameter in seismic safety evaluation, the shear-wave velocity of soil layer can best reflect the dynamic characteristics of site soil. The shear-wave velocity Vs30 may be a weak proxy in order to assess soil dynamic characteristics [31], according to the American code *Minimum Design Loads for Buildings and Other Structures* (ASCE/SEI 7-10), the European code *Design of Structures for Earthquake Resistance. Part 1: General Rules, Seismic Action and Rules for Buildings* (Eurocode 8), etc. According to the Chinese *Code for Seismic Design of Buildings* (GB50011-2010), the site category is determined according to the equivalent shear-wave velocity within 20 m below the ground surface (Vs20) and overburden thickness. The overburden thickness in the study area has been analyzed above, and the equivalent shear wave calculation is follows:

$$V_{se} = d_0/t \tag{4}$$

$$t = \sum_{i=1}^{n} \frac{d_i}{V_{si}} \tag{5}$$

where the calculated depth d_0 is the smaller of the overburden thickness and 20 m. Based on the borehole-measured wave velocity and microtremor inversion velocity model, the statistics of the calculated equivalent shear-wave velocity are shown in Table 1.

Table 1. Equivalent S-wave velocity, overburden thickness and engineering site category of each borehole and exploration point.

Study Area	Bore-Hole No.	Borehole In-Suit Test: Overburden Thickness h (m)	Equivalent S-Wave Velocity Vs20 (m/s)	Site Category	Microtremor Inversion Velocity Model: Exploration Point No.	Overburden Thickness h (m)	Equivalent S-Wave Velocity Vs20 (m/s)	Site Category	Overburden Error e_h	Velocity Error e_v
I He'an Line	zk43	51.8	173.9	III	H32	55.8	181.1	III	7.7%	4.1%
	zk47	55.0	178.3	III	H110	57.2	175.7	III	4.0%	1.5%
II Sha maoLine	zk10	>90.0	211.7	III	S33	93.7	195.8	III	-	7.5%
	zk11	>90.0	214.7	III	S95	101.0	192.8	III	-	10.2%
	zk12	>90.0	215.3	III	S151	107.6	204.5	III	-	5.0%

The errors between the equivalent shear-wave velocity estimated by the microtremor model of exploration points H32 and H110 of the He'an Line and the borehole-measured estimate are 4.1% and 1.5%, respectively, and those of exploration points S33, S95, and S151 of the Shamao Line are 7.5%, 10.2%, and 5.0%, respectively. For overburden thickness, the errors of the two exploration points of the He'an Line are 7.7% and 4.0%, respectively. The errors of the Shamao Line are counted temporarily, as the moderately-weathered bedrock roof is not exposed in the borehole. Although there is an error between the microtremor inversion model and borehole-measured data, it is small. Besides, the site classification in relevant specifications is relatively rough. So, the result of the microtremor survey is decided to be consistent with the borehole-measured one, both being site III.

The calculation formula of the error e between the two defined in the table is follows:

$$e = \frac{measured\ data - inversion\ data}{measured\ data} \times 100\% \tag{6}$$

With increasing requirements for earthquake prevention and disaster reduction, to predict seismic hazards in key areas, it is necessary to consider a wide range of regional site conditions. The continuous shear-wave velocity profiles obtained by microtremor survey can replace drilling to determine site category in some sites, which can reduce drilling workload to a certain extent.

4.4. Result Analysis

The He'an Line is 750 m long, with 151 exploration points. The pseudo two-dimensional profile of the apparent S-wave velocity is obtained through an inversion of the dispersion curve of each exploration point, as shown in Figure 8.

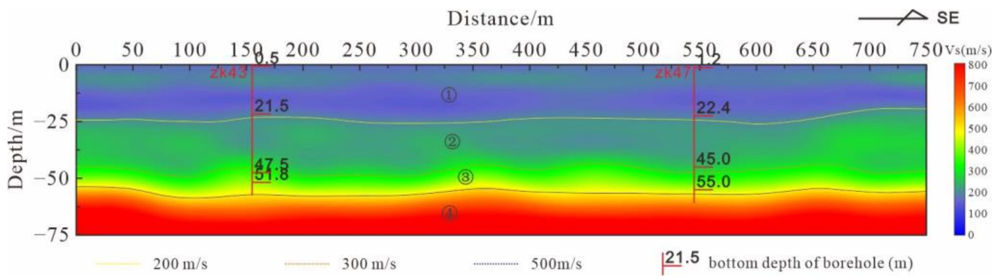

Figure 8. Microtremor inversion result of the He'an line in area I.

It can be seen from the inversion profile that the effective inversion depth is about 75 m. The apparent S-wave velocity of the profile is evenly distributed, horizontally continuous, and longitudinally with obvious increase and stratification. Generally, it can be divided into four layers. The apparent S-wave velocity interfaces are 200 m/s, 300 m/s, and 500 m/s, respectively. Two boreholes, zk43 and zk47, are distributed near the survey line mileage of 155 m and 545 m. According to the borehole data, the geological significance of the profile is as follows: the surface layer (① in Figure 8) is silty clay (plastic) and silty fine sand (slightly dense), the apparent S-wave velocity is less than 200 m/s, and the bottom depth varies between 19.2–26.2 m; the second layer (② in Figure 8) is silty fine sand (moderately dense) and medium sand (dense), the apparent S-wave velocity range is 200–300 m/s, and the bottom depth varies between 43.2–49.6 m; the third layer (③ in Figure 8) is sand mixed with pebbles and strongly-weathered conglomerate, the apparent S-wave velocity range is 300–500 m/s, and the bottom depth varies between 53.5–58.5 m; and the bottom layer (④ in Figure 8) is moderately-weathered conglomerate, and the apparent S-wave velocity is greater than 500 m/s.

The microtremor inversion data reveal that the deposit of each layer is relatively stable, the shear-wave velocity structure gradually increases, and the overburden thickness varies within the range of 53.5–58.5 m.

The Shamao Line is 800 m long, with 161 exploration points. The pseudo two-dimensional profile of the apparent S-wave velocity is shown in Figure 9.

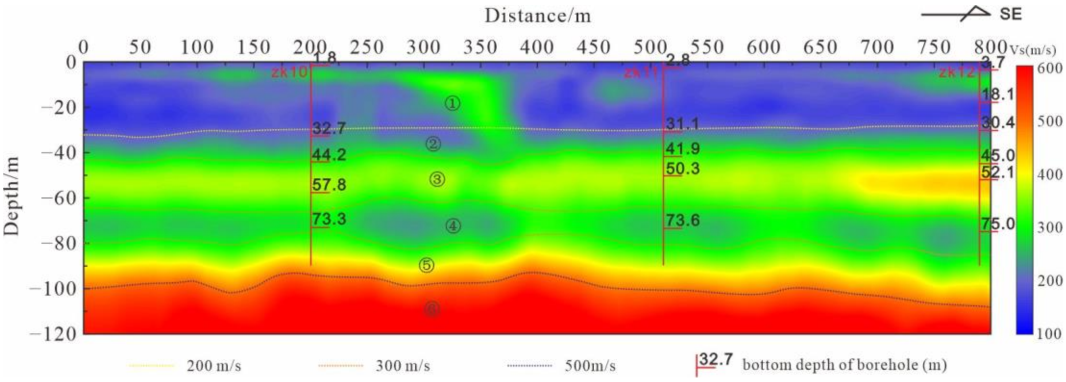

Figure 9. Microtremor inversion result of the Shamao line in area II.

It can be seen from the inversion profile that the effective inversion depth is about 120 m. The apparent S-wave velocity of the profile is relatively evenly distributed, horizontally continuous, and longitudinally with obvious stratification. Generally, it can be divided into six layers, of which there is a low-velocity weak interlayer near the depth of about 75 m. Three boreholes, zk10, zk11, and zk12, are distributed near the survey line mileage of 160 m, 470 m, and 750 m. According to the borehole data, the geological significance of the profile is as follows: the surface layer (① in Figure 9) is silty clay (soft plastic and plastic), the apparent S-wave velocity is less than 200 m/s, and the bottom depth varies between 27.9–33.7 m; the second layer (② in Figure 9) is silty fine sand (slightly-moderately dense), the apparent S-wave velocity range is 300–450 m/s, and the bottom depth varies between 38.3–45.9 m; the third layer (③ in Figure 9) is medium-coarse sand mixed with gravel (medium-dense), the apparent S-wave velocity range is 300–500 m/s, and the bottom depth varies between 59.8–67.7 m; the fourth layer (④ in Figure 9) is a low-velocity soft layer of silt mixed with silty clay (plastic), the apparent S-wave velocity is less than 300 m/s, and the layer thickness is about 17.5–23.0 m; the fifth layer(⑤ in Figure 9) is strongly-weathered argillaceous siltstone, the apparent S-wave velocity range is 300–500 m/s, and the bottom depth varies between 94.2–107.5 m and gradually becomes deeper along the SE direction; and the bottom layer (⑥ in Figure 9) is moderately-weathered argillaceous siltstone, and the apparent S-wave velocity is greater than 500 m/s.

The microtremor inversion data reveal that the bedrock surface gradually deepens along the SE direction, the deepest part of the profile is about 107.6 m, and there is a low-velocity weak layer (④ in Figure 9) on it, with a thickness of about 17.5–23.0 m. The deposit of the upper layers ①, ②, and ③ is relatively stable, and the bottom depth changes little.

5. Discussion

The physical and mechanical properties of weak interlayer are extremely feeble, especially when the underlying weak interlayer has certain thickness, the seismic response of the underground structure is more intense than that of the conventional uniform site conditions, which usually called local soil amplification. This adverse geological phenomenon is extremely harmful to major engineering constructions. At present, for the identification of weak interlayer, especially when the buried depth is large, such as 50–100 m, the non-destructive detection has not achieved good results. Although high-resolution seismic reflection exploration can identify the reflection horizon of the target layer, it is not applicable to all construction environments, such as noise and other environmental disturbances.

The apparent S-wave velocity profile obtained in this paper can clearly show the characteristics of velocity change of a stratum structure with weak interlayer, based on which key information, such as stratigraphic structure and depth, can be accurately depicted. This method has strong applicability and can also achieve good results in noisy urban environments. These research results could better guide the design and construction of buildings and provide reference for future treatment scheme, while providing decision-making reference for governments in geological disaster control and urban and rural planning.

6. Conclusions

In this paper, on the premise of fully understanding regional tectonic background and stratigraphic lithology, a measurement study is conducted on two typical stratigraphic models in the Wuhan area using the long-spread microtremor array method. Through fine processing of the original data and calibration in combination with borehole data, two measured 2D profiles within a length of 800 m of the microtremor apparent-S wave are obtained. The velocity interface showed in the profiles has obvious change trend in the horizontal direction, with very clear fluctuation state; in the longitudinal direction, the depth information is reliable and highly consistent with the borehole information, of which the details are as follows:

(1) In study area I, the velocity of the profile obtained through a measurement along the He'an Line increases gradually from the surface to a depth of 75 m, which, in terms of geology, matches the four layers exposed by the boreholes, namely silty clay, silty fine sand, sand mixed with pebbles, and moderately-weathered conglomerate; the apparent S-wave velocity ranges are less than 200 m/s, 200–300 m/s, 300–500 m/s, and greater than 500 m/s, respectively, which is consistent with the wave velocity results of the in situ test. The measured results of the conventional stratum well verify the correctness of the research method in this paper.

(2) In study area II, the velocity of the profile obtained through a measurement along the Shamao Line does not show an increasing trend from the surface to a depth of 120 m. There exists an obvious low-velocity interlayer between 60.0–82.0 m, which has never been seen in previous studies. The velocity of the low-velocity layer is about 200 m/s lower than that of the upper and lower strata. Through borehole verification, both zk10 and zk11 reveal the existence of weak strata within the depth between 50.3–73.6 m. The apparent shear-wave velocity obtained through the microtremor inversion is also consistent with the wave velocity test results, which further verifies the applicability of the research results of this paper to weak strata.

(3) Based on the microtremor inversion results, the overburden thickness and the equivalent shear-wave velocity can be estimated, and then the site category can be determined, which provides important seismic parameters for engineering site survey. Compared to the in situ test data, the error of overburden thickness and $Vs20$ of the two cases in this paper is about 10%, with the site category being both site III. Compared to drilling, with high efficiency, this method can help reduce the drilling workload to a certain extent, and the detection results could provide important basic data for regional seismic safety and seismic risk assessment of major projects in complex urban areas.

Author Contributions: Conceptualization, C.J. and S.L.; methodology, C.J.; software, C.J.; validation, S.L. and J.W.; formal analysis, C.J.; investigation, H.Z.; resources, H.Z.; data curation, C.J. and M.C.; writing—original draft preparation, C.J.; writing—review and editing, S.L.; visualization, C.J.; supervision, S.L.; project administration, C.J.; funding acquisition, S.L. and J.W. All authors have read and agreed to the published version of the manuscript.

Funding: This research was funded by the Scientific Research Fund from the Institute of Seismology, CEA and National Institute of Natural Hazards, Ministry of Emergency Management of China, grant number IS201926301; the Natural Science Foundation of Hebei Province, grant number D2020210009; and the Science and Technology Projects of Hebei Education Department, grant number BJ2021036.

Institutional Review Board Statement: Not applicable.

Informed Consent Statement: Not applicable.

Data Availability Statement: Not applicable.

Conflicts of Interest: The authors declare no conflict of interest.

References

1. Boaga, J.; Vignoli, G.; Cassiani, G. Shear wave profiles from surface wave inversion: The impact of uncertainty on seismic site response analysis. *J. Geophys. Eng.* **2011**, *8*, 162–174. [CrossRef]
2. Soupios, P.; Georgakopoulos, P.; Papadopoulos, N.; Saltas, V.; Andreadakis, A.; Vallianatos, F.; Sarris, A.; Makris, J. Use of engineering geophysics to investigate a site for a building foundation. *J. Geophys. Eng.* **2007**, *4*, 94–103. [CrossRef]
3. Wang, J.; Huang, J.; Min, H.; Wang, F.; Wang, Y.; Han, Z. Study on the Weak Interlayer Identification Method Based on Borehole Photo-Acoustic Combined Measurement: Application to a Landslide Case Study. *Appl. Sci.* **2022**, *12*, 10545. [CrossRef]
4. Lin, P.; Zheng, W.; Huang, B.; Zhang, H. Seismic Fortification Analysis of the Guoduo Gravity Dam in Tibet, China. *Shock Vib.* **2015**, *2015*, e396124. [CrossRef]
5. Xia, J.; Miller, R.D.; Park, C.B. Estimation of near-surface shear-wave velocity by inversion of Rayleigh waves. *Geophysics* **1999**, *64*, 691–700. [CrossRef]
6. Kim, K.Y.; Kim, W.J.; Park, Y.H. Inversion of Rayleigh-wave Dispersion Curves for Near-surface Shear-wave Velocities in Chuncheon Area. *Geophys. Geophys. Explor.* **2012**, *15*, 1–7. [CrossRef]
7. Park, C.B.; Miller, R.D.; Xia, J. Multichannel analysis of surface waves. *Geophysics* **1999**, *64*, 800–808. [CrossRef]
8. Mi, B.; Xia, J.; Shen, C.; Wang, L.; Hu, Y.; Cheng, F. Horizontal resolution of multichannel analysis of surface waves. *Geophysics* **2017**, *82*, EN51–EN66. [CrossRef]
9. You, Z.; Xu, P.; Qian, J.; Cao, L.; Du, Y.; Fu, Q. Frequency-Bessel Transform Based Microtremor Survey Method and Its Engineering Application. *Int. J. Environ. Res. Public Health* **2022**, *19*, 13484. [CrossRef]
10. Ávila-Barrientos, L.; Yegres-Herrera, L.A.; Flores-Estrella, H.; González-Fernández, A. Estimation of shallow VP and VS models in La Reforma Caldera, Baja California Sur, Mexico, using H/V ratios. Preliminary results. *J. Appl. Geophys.* **2022**, *204*, 104736. [CrossRef]
11. Cheng, F.; Xia, J.; Xu, Y.; Xu, Z.; Pan, Y. A new passive seismic method based on seismic interferometry and multichannel analysis of surface waves. *J. Appl. Geophys.* **2015**, *117*, 126–135. [CrossRef]
12. Okada, H. Theory of efficient array observations of microtremors with special reference to the SPAC method. *Explor. Geophys.* **2006**, *37*, 73–85. [CrossRef]
13. Karagoz, O.; Chimoto, K.; Citak, S.; Ozel, O.; Yamanaka, H.; Hatayama, K. Estimation of shallow S-wave velocity structure and site response characteristics by microtremor array measurements in Tekirdag region, NW Turkey. *Earth Planets Space* **2015**, *67*, 176. [CrossRef]
14. Tian, B.; Du, Y.; Jiang, H.; Zhang, R.; Zhang, J. Estimating the shear wave velocity structure above the fresh bedrock based on small scale microtremor observation array. *Bull. Eng. Geol. Environ.* **2020**, *79*, 2997–3006. [CrossRef]
15. Dai, K.; Liu, K.; Li, X.; You, Q.; Tang, H.; Xu, Q. Application of passive multichannel analysis of surface waves method at sites close to underground railways-Problems and a case study. *J. Appl. Geophys.* **2019**, *164*, 191–199. [CrossRef]
16. Ning, L.; Dai, T.; Liu, Y.; Xi, C.; Zhang, H.; Zhou, C. Application of multichannel analysis of passive surface waves method for fault investigation. *J. Appl. Geophys.* **2021**, *192*, 104382. [CrossRef]
17. Xu, P.; Shi, W.; Ling, S.; Guo, H.; Li, Z. Mapping spherically weathered "Boulders" using 2D microtremor profiling method: A case study along subway line 7 in Shenzhen. *Chin. J. Geophys.* **2012**, *55*, 2120–2128. [CrossRef]
18. Tian, B.; Xu, P.; Ling, S.; Du, J.; Xu, X.; Pang, Z. Application effectiveness of the microtremor survey method in the exploration of geothermal resources. *J. Geophys. Eng.* **2017**, *14*, 1283–1289. [CrossRef]
19. Huang, H.C.; Shih, T.H.; Hsu, C.T.; Wu, C.F. Estimation of Shear-Wave Velocity Structures in Taichung, Taiwan, Using Array Measurements of Microtremors. *Appl. Sci.* **2021**, *12*, 170. [CrossRef]
20. Wang, W.; Jin, C.; Luo, D.; Cai, Y.; Lin, S. Comprehensive Geophysical Measurement in Seismic Safety Evaluation: A Case Study of East Lake High-Tech Development Zone, China. *Sustainability* **2022**, *14*, 6307. [CrossRef]
21. Okada, H.; Suto, K. *The Microtremor Survey Method*; Society of Exploration Geophysicists: Houston, TX, USA, 2003.
22. Toksöz, M.N.; Lacoss, R.T. Microseisms: Mode structure and sources. *Science* **1968**, *159*, 872–873. [CrossRef] [PubMed]
23. Margaryan, S.; Yokoi, T.; Hayashi, K. Experiments on the stability of the spatial autocorrelation method (SPAC) and linear array methods and on the imaginary part of the SPAC coefficients as an indicator of data quality. *Explor. Geophys.* **2009**, *40*, 121–131. [CrossRef]
24. Aki, K. Space and time spectra of stationary stochastic waves, with special reference to microtremors. *Bull. Earthq. Res. Inst.* **1957**, *35*, 415–456.
25. Capon, J. High-resolution frequency-wavenumber spectrum analysis. *Proc. IEEE* **1969**, *57*, 1408–1418. [CrossRef]
26. Park, C.B.; Miller, R.D.; Xia, J.; Ivanov, J. Multichannel analysis of surface waves (MASW)—Active and passive methods. *Lead. Edge* **2007**, *26*, 60–64. [CrossRef]
27. Cheng, F.; Xia, J.; Luo, Y.; Xu, Z.; Wang, L.; Shen, C.; Liu, R.; Pan, Y.; Mi, B.; Hu, Y. Multichannel analysis of passive surface waves based on crosscorrelations. *Geophysics* **2016**, *81*, EN57–EN66. [CrossRef]

28. Liu, Y.; Xia, J.; Cheng, F.; Xi, C.; Shen, C.; Zhou, C. Pseudo-linear-array analysis of passive surface waves based on beamforming. *Geophys. J. Int.* **2020**, *221*, 640–650. [CrossRef]
29. Zhang, H.; Chen, X.; Zhang, H.; Xia, J. Dispersion measurement from ultra-short ambient noise using phase-weighted stacking in urban areas. *J. Appl. Geophys.* **2022**, *199*, 104587. [CrossRef]
30. Rosa-Cintas, S.; Galiana-Merino, J.J.; Molina-Palacios, S.; Rosa-Herranz, J.; García-Fernández, M.; Jiménez, M.J. Soil characterization in urban areas of the Bajo Segura Basin (Southeast Spain) using H/V, F–K and ESAC methods. *J. Appl. Geophys.* **2011**, *75*, 543–557. [CrossRef]
31. Vanzi, I.; Marano, G.C.; Monti, G.; Nuti, C. A synthetic formulation for the Italian seismic hazard and code implications for the seismic risk. *Soil Dyn. Earthq. Eng.* **2015**, *77*, 111–122. [CrossRef]